Available online at www.sciencedirect.com

ScienceDirect

Energy Procedia 92 (2016) 145 – 152

Energy Procedia

6th International Conference on Silicon Photovoltaics, SiliconPV 2016

# Evaluating depth distributions of dislocations in silicon wafers using micro-photoluminescence excitation spectroscopy

Hieu T. Nguyen*, Sieu Pheng Phang, and Daniel Macdonald

*Research School of Engineering, College of Engineering and Computer Science, The Australian National University, Canberra, ACT 2601, Australia*

**Abstract**

Combining micro-photoluminescence spectroscopy and photoluminescence excitation spectroscopy, we are able to observe the evolution of the luminescence spectra from crystalline silicon wafers under various excitation wavelengths. By interpreting the relative change of the luminescence spectra, we can detect and examine the distributions of the dislocations, as well as of the defects and impurities trapped around them, segregated at different depths below the wafer surface. We show that in multicrystalline silicon wafers, the dislocations and the trapped defects and impurities, formed during the ingot growth and cooling, are distributed throughout the wafer thickness, whereas those generated in monocrystalline wafers by a post-diffusion thermal treatment are located near the wafer surface.



Peer review by the scientific conference committee of SiliconPV 2016 under responsibility of PSE AG.

*Keywords:* Crystalline silicon; dislocations; photoluminescence (PL); photovoltaics.

## 1. Introduction

Photoluminescence spectroscopy (PLS) and photoluminescence imaging (PLI) have been demonstrated to be powerful characterization tools in silicon photovoltaics. Utilizing the advantages of these two techniques, the so-called hyperspectral PL imaging technique, which combines both PLS and PLI, has been employed to capture macroscopic PL images from multicrystalline silicon (mc-Si) wafers in both spatial and spectral dimensions [1,2].

* Corresponding author
*E-mail address:* hieu.nguyen@anu.edu.au



Peer review by the scientific conference committee of SiliconPV 2016 under responsibility of PSE AG.
doi:10.1016/j.egypro.2016.07.013

Therefore, macroscopic properties of different radiative recombination centers at various locations in mc-Si wafers can be investigated separately. However, due to the limited number of pixels from the camera employed to detect a large area on the wafers, the spatial resolution of this hyperspectral PL-based method is on the order of several hundred micrometers [1-2]. As a result, microscopic properties of submicron features in crystalline silicon (c-Si) wafers and solar cells have not been accessible via this technique.

Recently, courtesy of the high spatial resolution from confocal optics, micro-PLS (μPLS) has been utilized to investigate electronic and optical properties of many submicron features in c-Si wafers and solar cells, such as dislocations [3-6], metal precipitates [7], or damage induced by laser-doped processes [8-10]. In addition, photoluminescence excitation (PLE) spectroscopy, in which the relative PL intensity at a certain wavelength is monitored when the excitation energy is varied, is a powerful technique to study fundamental properties of silicon and defects, such as the optical band gap in degenerate silicon [11,12] or oxygen-related deep defects in irradiated silicon [13]. Recently, we have applied a technique combining μPLS and PLE to evaluate spatial distributions of structures and defects separated at different depths inside silicon wafers [14].

Dislocation sites are an important lifetime killer in silicon solar cells [15]. The dislocations themselves are not only an effective recombination channel for free carriers, but also act as trapping sites for other defects and impurities due to the local stress and strain around them. These trapped defects and impurities, in turn, reduce the free carrier concentrations even further. The dislocations and the trapped defects and impurities can be generated either during the crystal growth of an ingot, or in subsequent solar cell fabrication steps. Due to the different natures of these two processes, the spatial distributions of the dislocations and the trapped defects and impurities are expected to be different. Therefore, in this work, we apply our recently-developed μPLS-PLE technique [14] to study the distributions of dislocations and other defects generated during these two processes. Defects formed during mc-Si ingot growth are shown to be distributed uniformly depth-wise in the silicon wafers, whereas the process-induced defects are found to reside near the wafer surfaces.

## 2. Experimental details

The sample investigated in Section 3 is a <100>-oriented float-zone boron-doped c-Si wafer. It was first chemically etched in an $HF/HNO_3$ solution to remove saw damage. It went through a thermal diffusion process in a $BBr_3$ gas source at 1050 $^oC$ for 1 hour, and was then annealed in pure nitrogen gas at 1090 $^oC$ for 5 hours while the borosilicate glass (BSG) and boron-rich layer (BRL) were both still present on the wafer surfaces. These process steps are aimed to generate dislocations, along with other defects and impurities, located below the wafer surfaces. After that, any residual BSG and BRL layers were finally removed prior to performing the PL measurements.

The sample investigated in Section 4 is a directionally solidified, boron-doped p-type mc-Si wafer with a background doping of about $9\times10^{15}$ $cm^{-3}$. This wafer was also first chemically etched in an $HF/HNO_3$ solution to remove saw damage. After that, it was immersed in a defect etchant consisting of acetic/$HNO_3$/HF acids for 16 hours. The purpose of this second etching step is to delineate sub-grain boundaries (sub-GBs), which are otherwise not observable under a confocal microscope. These sub-GBs are known to have a high density of defects and impurities forming during the ingot growth and cooling process [5].

The setup of our μPLS system is described elsewhere [5,14]. The excitation light source is a supercontinuum laser (NKT SuperK Extreme EXR-20) with a tunable wavelength range from 490 nm to 2 μm. In this work, excitation wavelengths between 510 nm and 810 nm with a bandwidth of 10 nm were employed. The on-sample power was kept constant at 6 mW for all excitation wavelengths. The diameter of the illuminated spot on the samples varied between ~1 μm (for 510-nm excitation wavelength) and ~2 μm (for 810-nm excitation wavelength). The spectral response of the entire system was determined with a calibrated halogen-tungsten light source.

## 3. Dislocations and impurities distributed near the wafer surface

In this section, we apply the combined PLS-PLE technique to detect dislocations, as well as other defects and impurities, distributed near the wafer surface. Figure 1a shows the normalized PL spectra from the boron-diffused and annealed c-Si wafer, excited with different wavelengths at 79 K. There are 3 distinct components in the spectra. The first component is the Band-to-Band (BB) peak at ~1130 nm emitted from the underlying c-Si substrate. The

second component is the peak at ~1165 nm attributed to the heavily-doped layer near the surface. This second peak is also band-to-band luminescence, but shifted to longer wavelengths due to band-gap narrowing effects in the heavily-doped layer [16]. Therefore, we denoted it as Heavily-Doped Band-to-Band peak (HDBB). The HDBB peak is significantly broader than the BB peak due to the band filling and band tailing effects in heavily-doped silicon [17,18]. The third component is the deep-level luminescence at wavelengths beyond 1200 nm, emitted from defects and impurities induced by the post-diffusion thermal treatment.

In Figure 1a, the HDBB peak reduces significantly with increasing excitation wavelengths due to the reduced absorption fraction of the laser light in the heavily-doped layer. In addition, the two deep-level peaks display the same trend as the HDBB peak, initially suggesting that the defects and impurities are distributed near the wafer surface. However, there could be another possibility. The BB intensity is a quadratic function of the excess carrier density under high injection levels [19], while the deep-level intensities are less dependent on the excess carrier density [10]. Therefore, the reduction of the deep-level luminescence in Figure 1a (compared to the BB peak) could be due to the faster increment of the BB peak when the laser light penetrates more deeply into the substrate, in which case the surface recombination is reduced. To test this hypothesis, we compare the spectra in relative intensities, as depicted in Figure 1b and Figure 1c (a zoomed-in section of Figure 1b). The BB peak increases remarkably with increasing excitation wavelengths (Figure 1b), while the deep-level luminescence saturates (Figure 1c). These results also suggest that the observed defects and impurities are located near the surface.

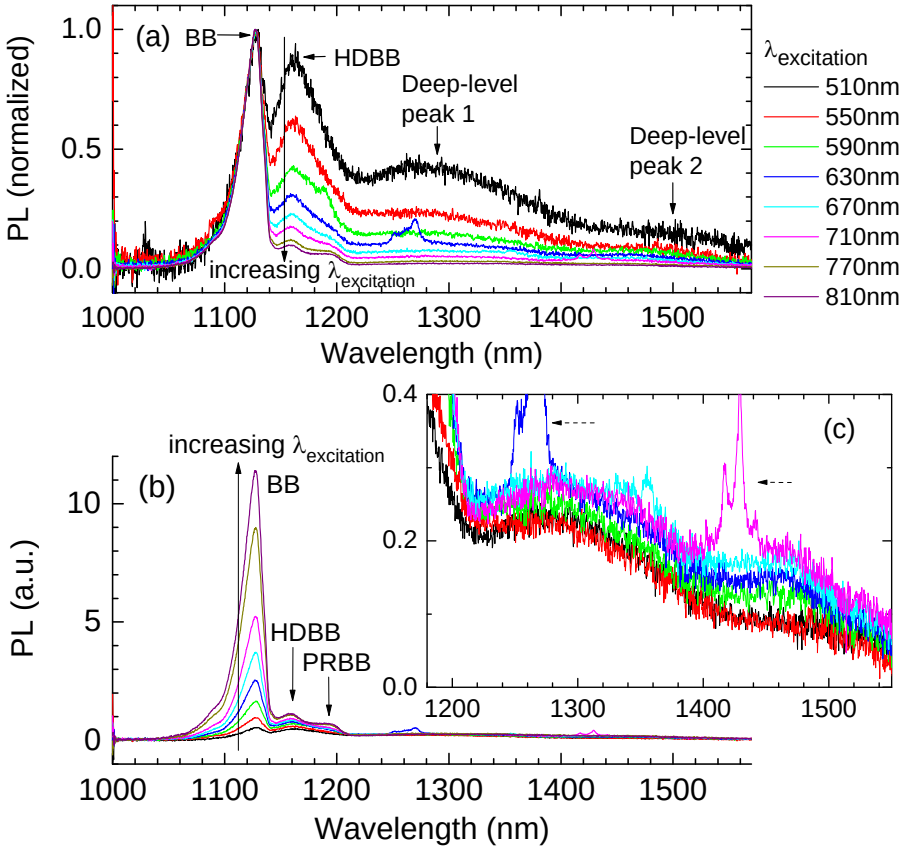


Fig. 1. PL spectra from the boron-diffused and annealed c-Si wafer, excited with different wavelengths at 79 K. The spectra were (a) normalized to the BB peak and (b) presented in relative intensities. (c) A zoom-in between 1180 and 1550nm of Figure 1b. The peak ~1200 nm is the phonon replica of the BB peak (denoted as PRBB in Figure 1b). The spurious peaks marked by broken-line arrows are artifacts due to the higher orders of the supercontinuum laser.

The very broad widths of these two deep-level peaks could be due to two reasons. The first reason is that, the doping profile is inhomogeneous across the diffused layer thickness. Thus, both deep-level peaks are, in fact, the aggregate PL emissions from different layers with different doping densities, which are shifted by varying amounts in energy due to changing band-gap narrowing. Another possibility is that, each of the two broad peaks could be possibly emitted from various defect and impurity centers locating near together inside the band gap rather than a single type of defects and impurities, and the PL emissions from these centers are also broadened due to the inhomogeneous doping profile. However, decomposing these two broad deep-level peaks into individual defect lines is difficult since these peaks are very broad and not well-defined.

Next, we continue examining the spatial distribution of the two deep-level luminescence peaks. In order to avoid the influence of the PL signal from the underlying substrate on our interpretation, we subtracted the BB component from the total spectra and normalized the resultant spectra to the HDBB peak, as depicted in Figure 2. Compared to deep-level peak 2, deep-level peak 1 is clearly suppressed with increasing excitation wavelengths, suggesting different origins and spatial distributions between the two deep-level peaks. Deep-level peak 1 is confined very near the surface while deep-level peak 2 is extended more deeply into the substrate.

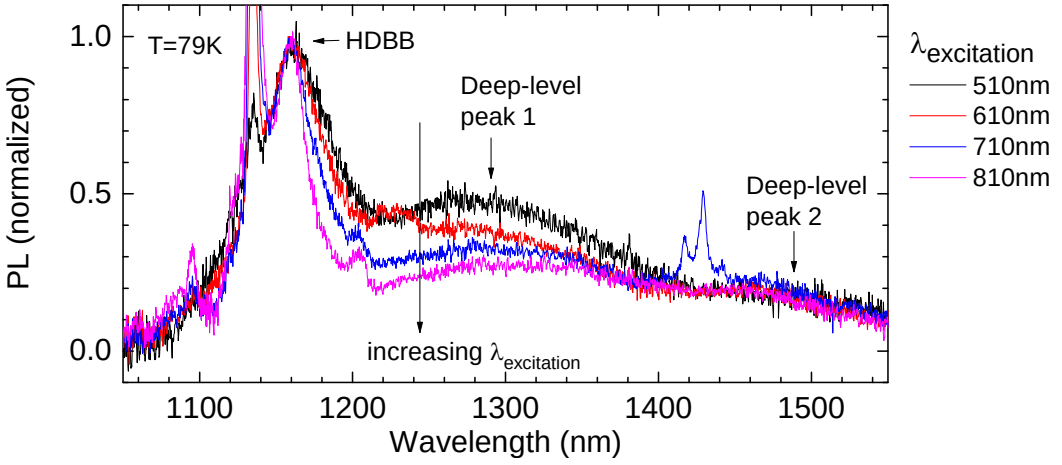


Fig. 2. PL spectra from the boron-diffused and annealed silicon wafer, excited with different wavelengths at 79 K. The BB peak from the c-Si substrate was subtracted from the original spectra, and the resultant spectra were normalized to the HDBB peak.

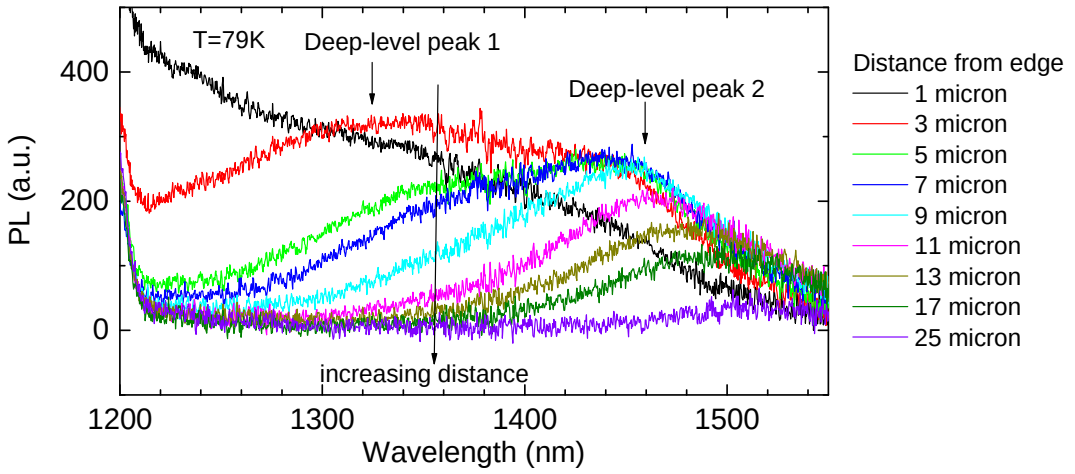


Fig. 3. PL spectra at different distances from the edge of the cross-sectional specimen (i.e. the original wafer surface) of the boron-diffused and anneal c-Si wafer. The excitation wavelength is 810 nm and the temperature is 79 K.

Now, we verify the findings on the spatial distributions of both these peaks mentioned above, using the PL spectra measured from a vertical cross-section of the boron-diffused and annealed c-Si wafer. Figure 3 plots the PL spectra at various distances from the edge of the cross-sectional specimen, i.e. the original wafer surface. Near the edge (e.g. the 3-micron curve), the intensities of both deep-level peak 1 and deep-level peak 2 are relatively high. Away from the edge of the cross-sectional specimen, deep-level peak 1's intensity is quickly diminished and eventually disappears. Meanwhile, deep-level peak 2 is still present up to a distance much further from the edge.

Furthermore, Figure 4 is a transmission electron microscope (TEM) two-beam bright-field image of the vertical cross-section. The micrograph reveals a dislocation band located about 3 microns below the surface. This dislocation band was formed during the post-diffusion thermal treatment. The dislocation band position coincides with the distance from the edge that yields the highest intensity of deep-level peak 1 (the 3-micron curve in Figure 3). Therefore, we suggest that deep-level peak 1 is likely to be related to the dislocations near the surface, while deep-level peak 2 could be attributed to the other defects and impurities trapped around the dislocation sites during the annealing and cooling process.

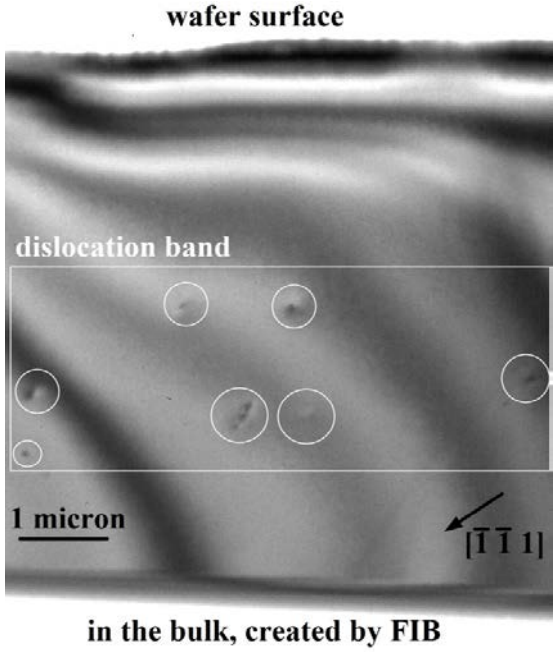


Fig. 4. TEM two-beam [-1-11] bright-field image of the (011) cross-section of the (100) boron-diffused and annealed c-Si wafer. The specimen was prepared by focus ion beam (FIB). The dislocations are marked with the white circles. The broad wavy features are bending contours due to the elastic bending of the thin TEM specimen.

## 4. Dislocations and impurities distributed depth-wise

In this section, we continue applying the combined PLS-PLE technique to assess dislocations and defects which are formed during the growth and cooling of a mc-Si ingot, rather than during the subsequent solar cell processing steps. In mc-Si wafers, dislocations are confined around small-angle grain boundaries or other sub-GBs, and are often decorated with other defects and impurities [3]. The dislocations themselves emit the so-called D3 and D4 lines around 1200 – 1300 nm [3-6], whereas the trapped defects and impurities are known to emit the so-called D1 and D2 lines between 1350 and 1600 nm [3-6].

Figure 5a shows the normalized PL spectra from a sub-GB of the mc-Si wafer with different excitation wavelengths at 79 K. Besides the BB peak from c-Si, we can observe deep-level luminescence peaks labeled as D4 and D3 (from dislocations) and D2 (from defects and impurities trapped around dislocations). In contrast to

Figure 1, the deep-level luminescence increases with increasing excitation wavelengths in Figure 5a. These results demonstrate that the dislocations are distributed depth-wise in the mc-Si wafer. Moreover, in Figure 5b, although the relative intensity of the defect luminescence increases, the relative BB intensity saturates. This behavior can be explained by the fact that the BB PL signal is limited by both the surface recombination and the defect density, in particular the density of dislocations in this case. Therefore, when the laser light penetrates more deeply into the wafer, although the effects of the surface recombination are suppressed, the deep-level channels still compete with the BB luminescence. We note that the D1 line is absent and the D2 line intensity is minimal in Figure 5, suggesting that the sub-GB investigated does not contains a high density of impurities and other defects, but the dislocations themselves.

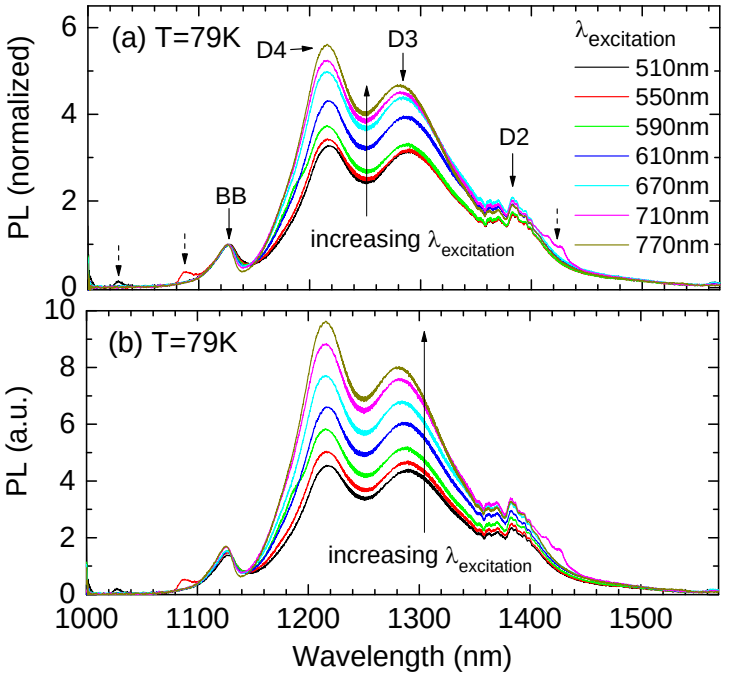


Fig. 5. PL spectra at a sub-GB, which gives strong dislocation luminescence, of the mc-Si wafer, excited with different wavelengths. The spectra were (a) normalized to the BB peak and (b) presented in relative scale. The spurious peaks marked by broken-line arrows are artifacts due to the higher orders of the supercontinuum laser.

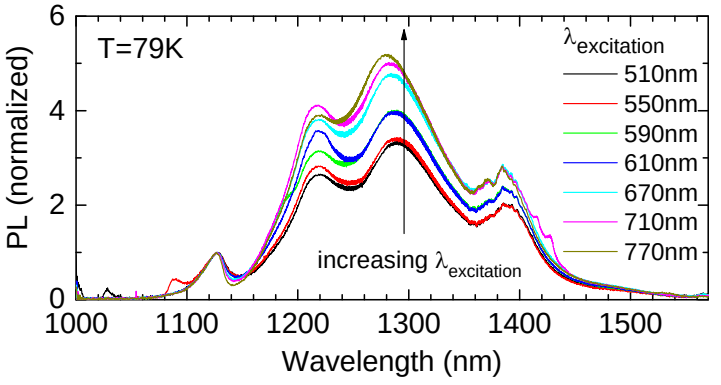


Fig. 6. PL spectra at the same sub-GB as in Figure 5, but measured from the other side of the mc-Si wafer, excited with different wavelengths.

Nevertheless, the increasing intensity of D3 and D4 with excitation wavelengths may imply a preferential increment of the dislocation density along the wafer thickness. To clarify this hypothesis, we repeated the PLE measurements on the same sub-GB, but from the other side of the wafer, and plotted the results in Figure 6. The increasing trend of D3 and D4 with increasing excitation wavelengths confirms that the higher intensity of D3 and D4 is due to a suppression of the surface recombination, rather than a higher dislocation density.

Finally, we show the results from another sub-GB, in which the dislocation sites are decorated with a high density of defects and impurities, causing strong D1 and D2 lines as depicted in Figure 7. The same as Figure 5, the dislocation luminescence intensity in Figure 7 increases with increasing excitation wavelengths. In addition, we also observe an increment of D1 and D2. The results from this figure demonstrate that, the defects and impurities are trapped around the dislocation sites during the ingot growth and cooling, and are also distributed throughout the wafer thickness.

Recently, Bauer *et al.* [20] have performed a detailed investigation on crystallographic structures of defects which are responsible for the strong recombination activities along sub-GBs in mc-Si solar cells. Combining electron beam induced current (EBIC) measurements and scanning transmission electron microscopy (STEM) images, these authors found a correlation between the increased recombination activities and the density of nonsplit Lomer dislocations along the sub-GBs. Moreover, they also showed that, the presence of partial dislocations and stacking faults at certain locations of the sub-GBs, in which perfect Lomer dislocations were absent, did not increase the EBIC contrast. Therefore, Lomer dislocations were suggested to be more detrimental to the final cell performance than partial dislocations and stacking faults. These findings can be compared to the properties of the D3 and D4 lines. The two lines have been confirmed to be due to the dislocations along the sub-GBs since the two lines are confined around the sub-GBs, in which the band-to-band intensity is found to be reduced significantly [3-5]. However, a detailed investigation on the microscopic structures of the dislocations around the sub-GBs studied in our work is required to clarify which types of dislocations emit the D3 and D4 lines. On the other hand, the D1 and D2 lines are still present at a distance far away from the sub-GBs, e.g. up to 80 μm from the sub-GBs in Ref. 5, and thus D1 and D2 are unlikely to be emitted directly from the dislocation networks at the sub-GBs.

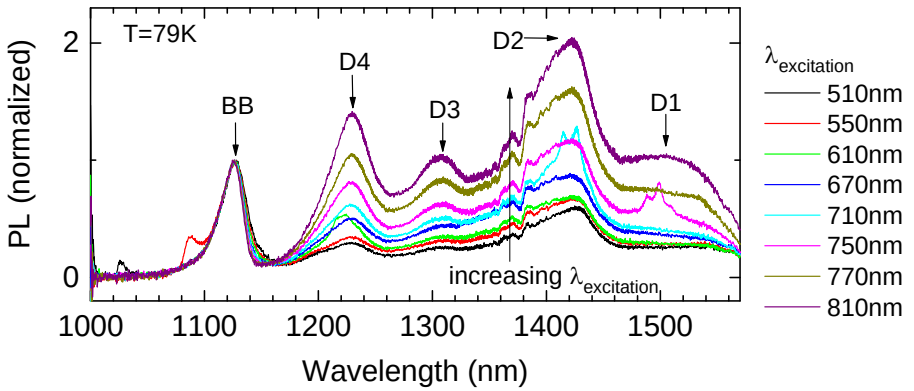


Fig. 7. Normalized PL spectra at a sub-GB, in which the dislocations sites are decorated with a high density of trapped defects and impurities, excited with different wavelengths.

## 5. Conclusion

We have applied the spectrally-resolved photoluminescence excitation spectroscopy technique to detect and assess the distributions of dislocations and other defects inside the silicon wafers. We have presented the results for two cases, between which the formations as well as distributions of dislocations and other defects are distinctly different. This method, in principle, can be applied for different structures and defects separated at different depths inside the silicon wafers.

## Acknowledgements

This work has been supported by the Australian Research Council (ARC) and the Australian Renewable Energy Agency (ARENA) through research grant RND009. The Australian National Fabrication Facility is acknowledged for providing access to some of the facilities used in this work. The authors are in debt to Prof. H. Tan for providing access to the spectroscopic equipment.

## References

[1] Olsen E, Flø AS. Spectral and spatially resolved imaging of photoluminescence in multicrystalline silicon wafers. Appl. Phys. Lett. 2011;99:011903-3.
[2] Lausch D, Mehl T, Petter K, Flø AS, Burud I, Olsen E. Classification of crystal defects in multicrystalline silicon solar cells and wafer using spectrally and spatially resolved photoluminescence. J. Appl. Phys. 2016;119:054501-6.
[3] Tajima M, Iwata Y, Okayama F, Toyota H, Onodera H, Sekiguchi T. Deep-level photoluminescence due to dislocations and oxygen precipitates in multicrystalline Si. J. Appl. Phys. 2012;111:113523-6.
[4] Tajima M. Spectroscopy and topography of deep-level luminescence in photovoltaic silicon. IEEE Journal of Photovoltatics 2014;4:1452-1458.
[5] Nguyen HT, Rougieux FE, Wang F, Tan H, Macdonald D. Micrometer-scale deep-level spectral photoluminescence from dislocations in multicrystalline silicon. IEEE Journal of Photovoltaics 2015;5:799-804.
[6] Nguyen HT, Rougieux FE, Wang F, Macdonald D. Effects of solar cell processing steps on dislocation luminescence in multicrystalline silicon. Energy Procedia 2015;77:619-625.
[7] Gundel P, Schubert MC, Kwapil W, Schön J, Reiche M, Savin H, Yli-Koski M, Sans JA, Martinez-Criado G, Seifert W, Warta W, Weber ER. Micro-photoluminescence spectroscopy on metal precipitates in silicon. Physica Status Solidi – Rapid Research Letters 2009;3:230-232.
[8] Woehl R, Gundel P, Krause J, Rühle K, Heinz FD, Rauer M, Schmiga C, Schubert MC, Warta W, Biro D. Evaluating the aluminum-alloyed p+-layer of silicon solar cells by emitter saturation current density and optical microspectroscopy measurements. IEEE Trans. Elec. Devices 2011;58:441-447.
[9] Roigé A, Alvarez J, Kleider JP, Martin I, Alcubilla R, Vega LF. Microscale spatially resolved characterization of highly doped regions in laser-fired contacts for high-efficiency crystalline Si solar cells. IEEE Journal of Photovoltatics 2015;5:545-551.
[10] Nguyen HT, Han Y, Ernst M, Fell A, Franklin E, Macdonald D. Dislocations in laser-doped silicon detected by micro-photoluminescence spectroscopy. Appl. Phys. Lett. 2015;107:022101-5.
[11] Wagner J. Photoluminescence and excitation spectroscopy in heavily doped n- and p-type silicon. Phys. Rev. B 1984;29:2002-2009.
[12] Wagner J. Heavily doped silicon studied by luminescence and selective absorption. Solid-State Electronics 1985;28:25-30.
[13] Wagner J, Thonke K, Sauer R. Excitation spectroscopy on the 0.79-eV (C) line defect in irradiated silicon. Phys. Rev. B 1984;29:7051-7053.
[14] Nguyen HT, Phang SP, Wong-Leung J, Macdonald D. Photoluminescence excitation spectroscopy of diffused layers on crystalline silicon wafers. IEEE Journal of Photovoltaics 2016;6:746-753.
[15] Sopori B, Rupnowski P, Mehta V, Budhraja V, Johnston S, Call N, Mountinho H, Al-Jassim M, Shaikh A, Seacrist M, Carlson D. Performance limitations of mc-si solar cells caused by defect clusters. ECS Transactions 2009;18:1049-1058.
[16] Nguyen HT, Yan D, Wang F, Zheng P, Han Y, Macdonald D. Micro-photoluminescence spectroscopy on heavily-doped layers of silicon solar cells. Physica Status Solidi – Rapid Research Letters 2015;9:230-235.
[17] Dumke WP. Comparison of band-gap shrinkage observed in luminescence from n+-si with that from transport and optical absorption measurements. Appl. Phys. Lett. 1983;42:196-198.
[18] Schmid PE, Thewalt MLW, Dumke WP. Photoluminescence in heavily doped Si:B and Si:As. Solid State Communications 1981;38:1091-1093.
[19]Nguyen HT, Rougieux FE, Baker-Finch SC, Macdonald D. Impact of carrier profile and rear-side reflection on photoluminescence spectra in planar crystalline silicon wafers at different temperatures. IEEE Journal of Photovoltaics 2015;5:77-81.
[20] Bauer J, Hähnel A, Werner P, Zakharov N, Blumtritt H, Zuschlag A, Breitenstein O. Recombination at Lomer dislocations in multicrystalline silicon for solar cell. IEEE Journal of Photovoltaics 2016;6:100-110.